

# 3D Shape of Specular Surface Measurement Using Five Degrees of Freedom Camera System

KHAIRI YUSUF, PRASETYO EDI and AMIR RADZI ABDUL GHANI

Department of Engineering Design and Manufacture

Faculty of Engineering, University of Malaya

50603 Kuala Lumpur

MALAYSIA

khairiyusuf@um.edu.my

*Abstract* : In this report, we describe a new method in obtaining a 3D shape of specular surface by using five degrees of freedom (5-DOF) camera. We use the principle that the normal vectors of the surface are extracted by aligning the camera axis and the surface normal vector. From the normal vector data, the shape of the surface is reconstructed. After the flat and the ball surface, the objects of the research are continued to convex and concave specular surface. The convex object is an automobile glass window, where in this object we show that the back reflection of a parallel surface of a thin glass can be eliminated. In the concave object we have a limitation that the radius of object is not smaller than twice of the nearest distance from the camera to the surface. The result shows that the methodology improves the 3-D shape of object measurement with good accuracy.

*Key-Words*: - shape reconstruction, pattern recognition, computer vision, image processing, five degrees of freedom camera, specular surface, normal vector, robotics.

## 1 Introduction

Specular surface has become interesting object since it is used widely especially in glass and metal industries. Besides that, many industrial materials are made of metal and have strong specularly and little diffuse reflection. Moreover, many practical tasks in robot vision and inspection require interpretation of images of specular or shiny surfaces.[1][2].

Several methods of obtaining the shape of a surface have been proposed such as multiple view, slit ray projection, moiré method, shape from shading and some of them are widely used in practical applications. An approach utilizes graded illumination fields to illuminate the surface has been proposed by Ikeuchi[1]. It uses the assumption that from a distant source and known object position, the angular relation between an observed reflected brightness and the position in the source field with that brightness could be used to derive surface orientation. This approach requires measurement of reflected brightness with sufficient accuracy to isolate a particular position in the source field. It uses the reflectance map and photometrics stereo.

Sanderson et. al. [2] proposed an approach of structured highlight to obtain the 3-D shape of specular surface. This approach uses multiple point

light sources and images the resulting highlight pattern reflected from the surface. It uses a spherical array of fixed point sources to scan all possible position and direction of incident light rays relative to a fixed camera. It is assumed that the point source are distant from the surface, that the surface is at a fixed reference height, and the extent of the surface from the origin is much smaller than the distance to the source. Such that the angle of incidence of illumination is determined only by the position of the source and does not depend on the relative position of illumination of the surface.

Babu et al. [3] uses a specular surface model to estimate orientation of an extended planar surface based on estimation of parameters in the shading model using contours of constant brightness in the image. This approach utilizes a parallel source and perspective camera model so that observed brightness of reflected illumination depends on surface position relative to the camera axis.

Schulz [4] showed some simulation of retrieving shape information from multiple images of a specular surface under natural lighting condition. The technique which is known as specular surface stereo consist of two parts, that are: a surface orientation procedure that computes the gradient at a point on the surface by minimizing the difference between observed and synthesized irradiance value, and a surface propagation procedure that retrieves

the shape of whole surface. The method is still in consideration since additional factors must be included in the image synthesis and illumination models if the method is applied to the real world.

This research conducting a new method of obtaining the shape of specular surface by extracting the surface normal vectors based on the reflection theorem and image processing. A 5-DOF camera is used to obtain the normal vector by scanning the alignment between the incident and reflected rays. A LED(Light Emitting Diode) is placed on the camera axis to give an incident ray to the surface. The camera axis is assumed intersects the center of image plane, hence, the alignment is reached when the reflected images coincide with the center of image plane. The location of the lens center and the direction of the camera axis on the aligning condition is recorded as the normal of the surface. From the normal vector data, the shape of the surface is reconstructed. This reconstruction gives a limitation in application that is used only to a smooth curve of object with no hole.

In the previous work we had verified the flat surface object and the convex surface object. The research is continued with examining a convex and a concave surface. At this time, the convex surface has a back surface reflection (like an automobile glass window) and has the limitation that the gradients at each corresponding points on both surfaces should be parallel. For a concave object, it also has a limitation that the radius of the surface is not smaller than twice of the nearest distance from the camera to the surface, where the camera still be able to receive the image in focus.

## 2 Principle

### 2.1 Extracting the Normal vector.

A specular surface always reflects the incident ray in the same angle. The normal vector at that point on a surface can be found if the incident and reflected angles are  $0^\circ$  or the incident ray align with the reflected ray. A simple camera model (see Fig. 1) has a camera axis with the center of image and the lens center on the camera axis. Since the gradient of a specular surface at a point is not directly perpendicular to the incident ray, the camera must be panned, tilted and moved in three coordinate axes to satisfy the alignment. Figure 2 shows the formation of an image of a single point, denoted by

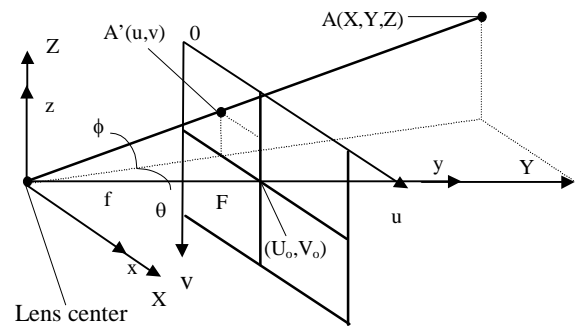


Fig.1. A simple camera model.

A, which has the coordinates  $(X, Y, Z)$ . The coordinates of A in the image are  $A'(x_A, z_A)$ , where

$$x_A = f \frac{X}{Y} ; \quad z_A = f \frac{Z}{Y} ; \quad (1)$$

Y is called the depth of A, which measured from the lens to the object. The distance from the lens to the image plane is denoted by f, the focal length. In the image coordinate system,  $A'(x_A, z_A)$  becomes  $A'(u, v)$ , after converting x and z by scale factor  $\alpha$  to u and  $\beta$  to v as follows

$$u = U_o + x_A \alpha \text{ (pixels)}; \quad v = V_o - z_A \beta ; \quad (2)$$

where  $\alpha, \beta$  in pixel/mm.

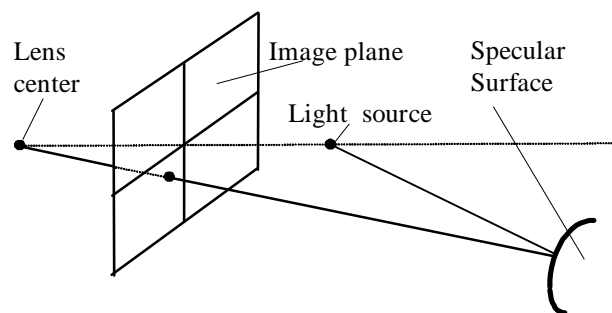


Fig. 2. Light source and Viewer

To get the normal vector, the image of point A must be moved to the center of image plane  $(U_o, V_o)$ . As shown in Fig. 3, the camera must be panned and tilted as much as :

$$\theta = \tan^{-1}((U_o - u)/F) ; \quad \phi = \tan^{-1}((V_o - v)/F) ; \quad (3)$$

where  $F = f\alpha$  (pixels),  $\theta$  is the pan angle, and  $\phi$  is the tilt angle.

We can express the normal line of a point on the specular surface as follows.

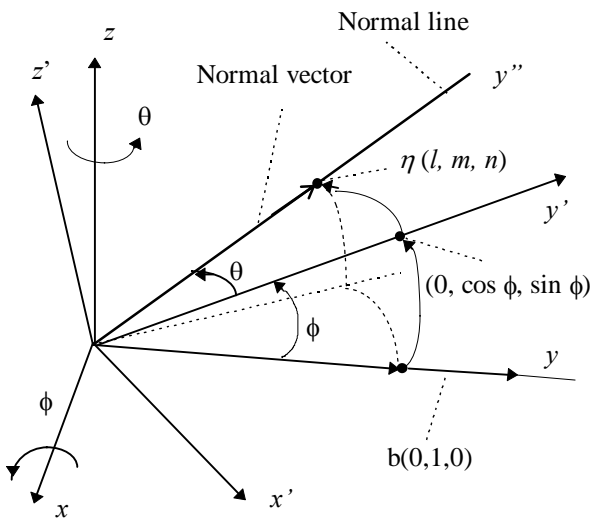


Fig. 3. Pan and tilt Angle.

$$\frac{y - y_c}{m} = \frac{x - x_c}{l} = \frac{z - z_c}{n} \tag{4}$$

$x_c, y_c, z_c$ , are the coordinates of a point on the normal line and  $l, m, n$  are the direction number of the normal line. We can derive that

$$\begin{aligned} l &= m \tan \theta \\ n &= m \tan \theta / \cos \phi \end{aligned} \tag{5}$$

**2.2 Shape Reconstruction.**

Reconstruction of the shape begins with the assumption that the shape is smooth otherwise we can not determine the shape of object from the surface normal vectors. Since there are infinite number of surfaces have the same normal vectors, the shape of object can not directly be reconstructed from the extracted normal vectors. This problem is solved by knowing at least one point coordinates on the surface as a starting point to lead the reconstruction. Cubic polynomial function of a surface shape is used here and expressed as follows :

$$y = \alpha_0 + \alpha_1 x + \alpha_2 x^2 + \alpha_3 x^3 + \alpha_4 z + \alpha_5 xz + \alpha_6 x^2 z + \alpha_7 z^2 + \alpha_8 xz^2 + \alpha_9 z^3 \tag{6}$$

The partial derivatives of this surface function is related to the components of surface normals, that are :

$$\frac{\partial y}{\partial x} = p; \frac{\partial y}{\partial z} = q \text{ where } p = -\frac{l}{m}; q = -\frac{n}{m} \tag{7}$$

Differentiation of eq. (6) with respect to  $x$  and  $z$  are

$$\frac{\partial y}{\partial x} = \alpha_1 + 2\alpha_2 x + 3\alpha_3 x^2 + \alpha_5 z + 2\alpha_6 xz + \alpha_8 z^2 \tag{8}$$

$$\frac{\partial y}{\partial z} = \alpha_4 + \alpha_5 x + \alpha_6 x^2 + 2\alpha_7 z + 2\alpha_8 xz + 3\alpha_9 z^2 \tag{9}$$

Eq. (7), (8), and (9) give

$$-\frac{l}{m} = \alpha_1 + 2\alpha_2 x + 3\alpha_3 x^2 + \alpha_5 z + 2\alpha_6 xz + \alpha_8 z^2 \tag{10}$$

$$-\frac{n}{m} = \alpha_4 + \alpha_5 x + \alpha_6 x^2 + 2\alpha_7 z + 2\alpha_8 xz + 3\alpha_9 z^2 \tag{11}$$

By using eq. (10) and (11), a procedure of reconstruction can be made.

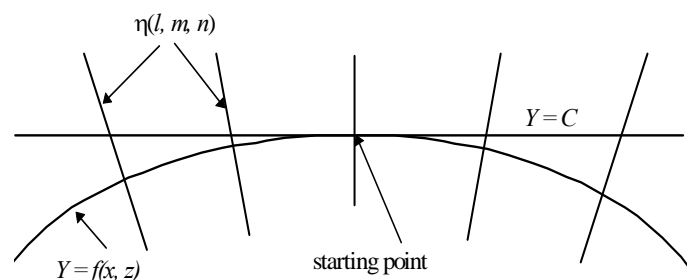


Fig. 4. Reconstruction of the shape.

As shown in Fig. 4 (two-dimensional view), a plane which is perpendicular to the  $Y$ -axis and passing through the starting point, is made. The equation of the plane can be written as

$$y = f(x_o, y_o, z_o) + \frac{\partial y}{\partial x}(x - x_o) + \frac{\partial y}{\partial z}(z - z_o) \tag{12}$$

$(x_o, y_o, z_o)$  is the starting point,

$\frac{\partial y}{\partial x}$  is the gradient of the function (6) in the  $x$  direction,

$\frac{\partial y}{\partial z}$  is the gradient of the function (6) in the  $z$  direction.

Since this plane is perpendicular to the  $Y$ -axis, the

plane equation becomes simple as,

$$Y = C \tag{13}$$

where  $C$  is the  $y$  coordinate of the starting point.

The intersection points between the normal line and the plane and the gradient at each point can easily be obtained, while the coefficient direction of the normal line are available. These are the requirements of reconstructing the shape.

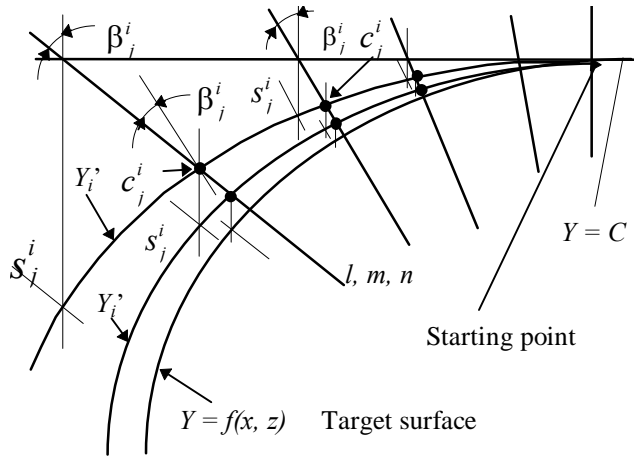


Fig. 5. Reconstruction of the Shape.

As shown more detail in Fig. 5, the reconstruction is started by a plane data (coordinates and directions), where the plane data contains the intersection points between the measured normal vector and the plane surface. The difference angle  $\beta_j^i$  (in  $X$ - $Y$  plane) and  $\gamma_j^i$  (in  $Z$ - $Y$  plane) between the measured normals and the plane normals is minimized. It is done by inputting the value of  $x$  and  $z$  of intersection points to the eq.(10) and (11). We will get the value of  $\alpha_i$ . This value then is used in eq.(6) and the starting point to get the first curve of  $Y'$ , where with coordinates  $x$  and  $z$  in the  $Y'$  curve is  $s_j^i$ . In other word, we get the  $Y'$  curve through  $s_j^i$ . These  $Y'$  curve has the intersection points with the measured normals at  $c_j^i$ . These points coordinates, the normals of the curve  $Y'$  and the angle  $\beta_j^i$  at these points can be calculated. Then the next differences minimization using the  $Y'$  curve and the measured normals can be done with the same procedure. This iteration is done until the target curve is found and the stop condition is achieved ( $\Sigma \beta_j^i$  and  $\Sigma \gamma_j^i < \text{small number } \epsilon$ ).

The differences between the measured normal direction  $(l,m,n)$  and the normal direction of the plane data is

$$\begin{aligned} \epsilon &= \sum_i \sum_j \left[ \left( \frac{\partial y}{\partial x} - \left(-\frac{l}{m}\right) \right)^2 + \left( \frac{\partial y}{\partial z} - \left(-\frac{n}{m}\right) \right)^2 \right] \\ \epsilon &= \sum_i \sum_j [(p-u)^2 + (q-v)^2] \end{aligned} \tag{14}$$

$$\begin{aligned} \text{where } p &= \frac{\partial y}{\partial x} ; q = \frac{\partial y}{\partial z} ; \\ u &= -\frac{l}{m} ; v = -\frac{n}{m} ; \end{aligned} \tag{15}$$

Minimization :

$$\frac{\partial \epsilon}{\partial \alpha_i} = 0 \quad (i = 0 \dots 9) \tag{16}$$

$$\frac{\partial \epsilon}{\partial \alpha_1} = 0, \quad \sum_i \sum_j 2[(p_{ij} - u_{ij})] = 0 ; \quad \frac{\partial \epsilon}{\partial \alpha_2} = 0,$$

$$\sum_i \sum_j 2[(p_{ij} - u_{ij})]2x_{ij} = 0;$$

$$\frac{\partial \epsilon}{\partial \alpha_3} = 0, \quad \sum_i \sum_j 2[(p_{ij} - u_{ij})]3x_{ij} = 0;$$

$$\frac{\partial \epsilon}{\partial \alpha_4} = 0, \quad \sum_i \sum_j 2[(q_{ij} - v_{ij})] = 0 ;$$

$$\frac{\partial \epsilon}{\partial \alpha_5} = 0,$$

$$\sum_i \sum_j [2(p_{ij} - u_{ij})z_{ij} + 2(q_{ij} - v_{ij})x_{ij}] = 0;$$

$$\frac{\partial \epsilon}{\partial \alpha_6} = 0,$$

$$\sum_i \sum_j [2(p_{ij} - u_{ij})2x_{ij}z_{ij} + 2(q_{ij} - v_{ij})x_{ij}^2] = 0 ;$$

$$\frac{\partial \epsilon}{\partial \alpha_7} = 0, \quad \sum_i \sum_j 2[(q_{ij} - v_{ij})]2z_{ij} = 0 ;$$

$$\frac{\partial \varepsilon}{\partial \alpha_8} = 0 ,$$

$$\sum_i \sum_j [2(p_{ij} - u_{ij})z_{ij}^2 + 2(q_{ij} - v_{ij})2x_{ij}y_{ij}] = 0 ;$$

$$\frac{\partial \varepsilon}{\partial \alpha_9} = 0 , \quad \sum_i \sum_j 2[(q_{ij} - u_{ij})]3z_{ij}^2 = 0 ;$$

Solution of  $\frac{\partial \varepsilon}{\partial \alpha_k} = 0$  ( $k = 0, \dots, 9$ ) can be written as the following simultaneous equation.

$$A^T A \alpha = A^T v \tag{17}$$

where

$$A = \begin{bmatrix} 1 & 2x_1 & 3x_1^2 & 0 & z_1 & 2x_1z_1 & 0 & z_1^2 & 0 \\ 0 & 0 & 0 & 1 & x_1 & x_1^2 & 2z_1 & 2x_1z_1 & 3z_1^2 \\ \cdot & \cdot & \cdot & \cdot & \cdot & \cdot & \cdot & \cdot & \cdot \\ \cdot & \cdot & \cdot & \cdot & \cdot & \cdot & \cdot & \cdot & \cdot \\ \cdot & \cdot & \cdot & \cdot & \cdot & \cdot & \cdot & \cdot & \cdot \\ \cdot & \cdot & \cdot & \cdot & \cdot & \cdot & \cdot & \cdot & \cdot \\ \cdot & \cdot & \cdot & \cdot & \cdot & \cdot & \cdot & \cdot & \cdot \\ 1 & 2x_n & 3x_n^2 & 0 & z_n & 2x_nz_n & 0 & z_n^2 & 0 \\ 0 & 0 & 0 & 1 & x_n & x_n^2 & 2z_n & 2x_nz_n & 3z_n^2 \end{bmatrix}$$

$$v = \begin{bmatrix} u_1 \\ v_1 \\ \cdot \\ \cdot \\ \cdot \\ \cdot \\ \cdot \\ u_n \\ v_n \end{bmatrix}, \quad \alpha = \begin{bmatrix} \alpha_1 \\ \alpha_2 \\ \cdot \\ \cdot \\ \cdot \\ \cdot \\ \cdot \\ \alpha_9 \end{bmatrix}$$

The equation means that approximate value of the coefficients are obtained in a sense of least mean square or regression [11].

### 2.3 Reconstruction sequence.

The intersection points are belong to several shapes of the surface, however, since a known point is included in the input data, the iteration will lead to an appropriate curve. However, the reconstruction is not done directly using all the normal vector since that way can not achieved an approximate shape of the surface. It is done in a piecewise reconstruction patch by patch. At every patch, to solve eq. (6), 5 points are need-

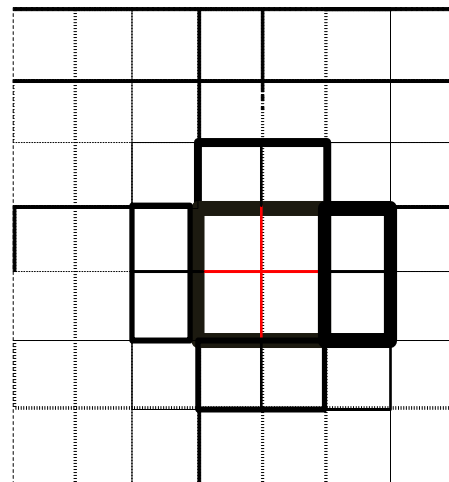
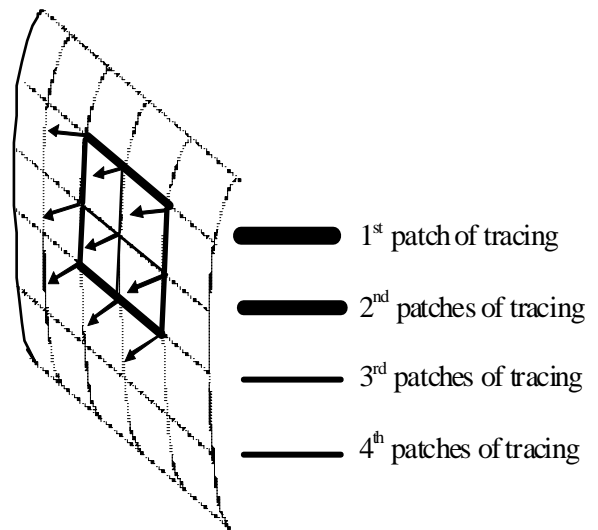


Fig. 6. Reconstruction Sequences. ed, otherwise the column vector of A are not linearly independent. In our method, we use 9 points included in 3 x 3 square matrix. All the normal vectors are traced patch by patch on the

surface carefully in a sequence as shown in Fig.6.

### 3.4 Reconstruction error.

In this reconstruction technique, some errors may occur because of two things that are, the difference in surface function, and the error of measured normal vectors. The first kind of error may occur because the surface function can not be approached precisely by a polynomial function. For example, a cylindrical surface can not be achieved precisely by a polynomial function although it can be changed into a polynomial function by Taylor series. Since we used the bicubic polynomial function, the higher order of the series will cause the error. However, this kind of error is not significant and always in the range of tolerance. Below a simulation of the first error is shown.

Say that there are two kinds of surface with the function as

$$y = ax^2, \quad \text{for every } z,$$

and

$$y^2 + x^2 = r^2, \text{ or } y = \sqrt{r^2 - x^2} \text{ for every } z.$$

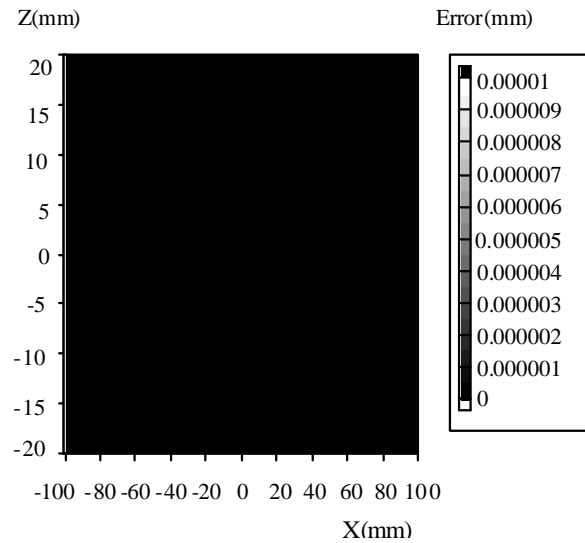
Consider that, both of surface have a set of ideal normal vector (l, m, n) which is calculated as

$$-\frac{l}{m} = \frac{\partial y}{\partial x}, \quad n = 0.0$$

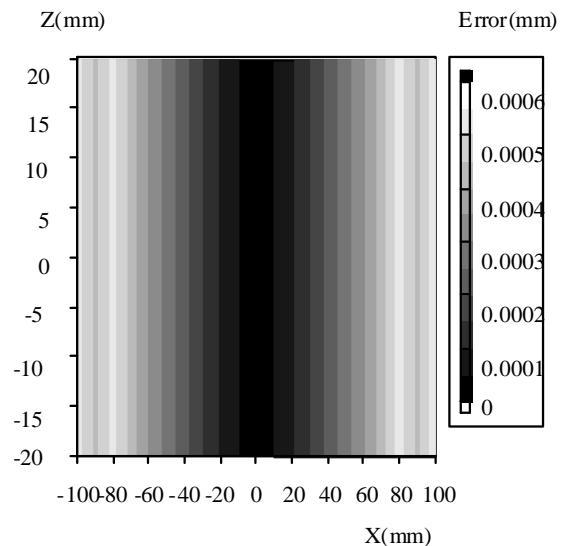
where  $l^2 + m^2 + n^2 = 1$ , such that

$$m = \frac{1}{\sqrt{\left(\frac{\partial y}{\partial x}\right)^2 + 1}}, \text{ and } l = -m \frac{\partial y}{\partial x}.$$

The first surface can be reconstructed from the normal vector precisely with no error as shown in Fig. 7.a, while the second reconstructed surface has some error as shown in Fig. 7.b.



(a)



(b)

Fig. 7 First Reconstruction Error .

The second kind of error occurs because of the error of normal vector. However, the normal vector error does not cause the propagation error. Superposition of normal vector error makes the error of reconstruction stable around some value. It can be shown by the following simulation.

The simple surface function of  $y = ax^2$  for every  $z$  is again used to get easy understanding. As presented before, reconstruction of this surface from its normal vector has no error. Here three kinds of normal vector sets are presented. The first set as shown in Fig. 8(a) contains error of  $+0.01^\circ$  for the

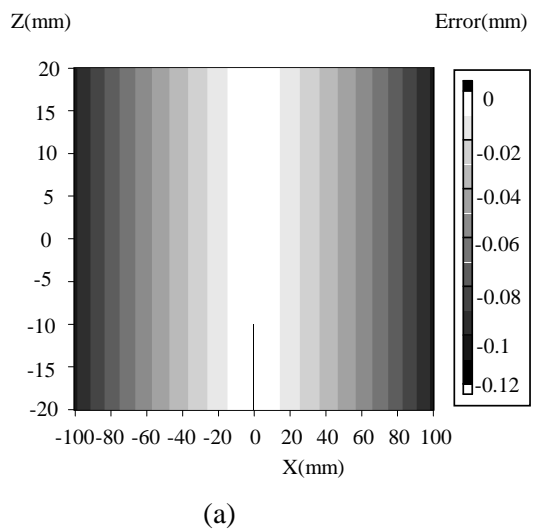
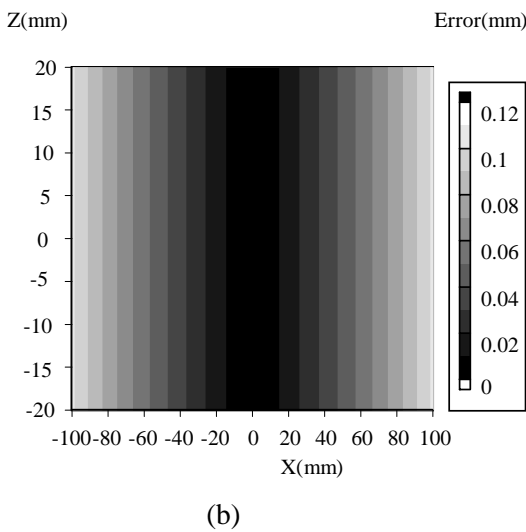
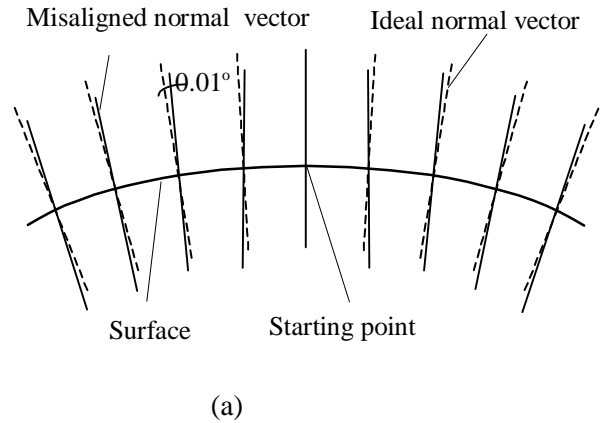
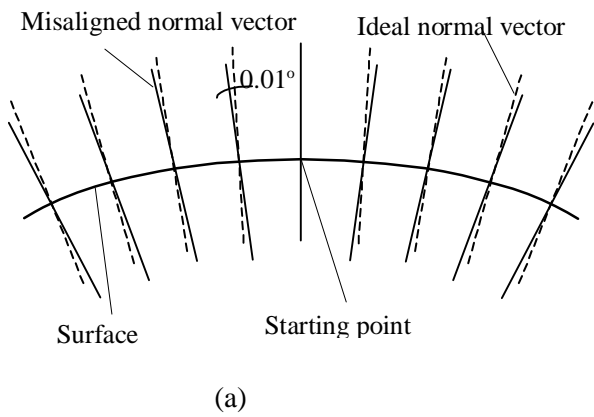


Fig. 8 (a)  $0.01^\circ$  (exaggerated) error to the left and right of the normal vector at the left and right of the starting point, and (b) its reconstruction error.

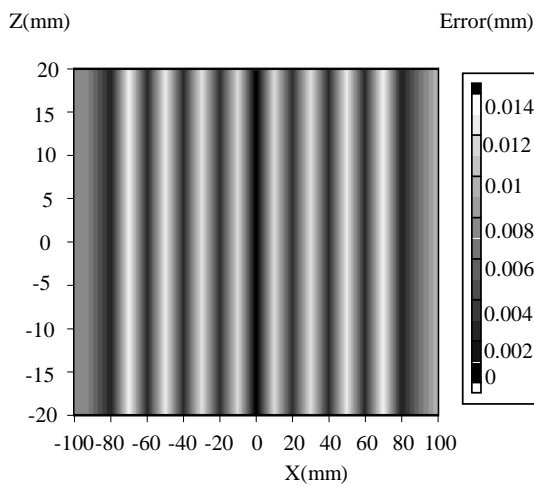
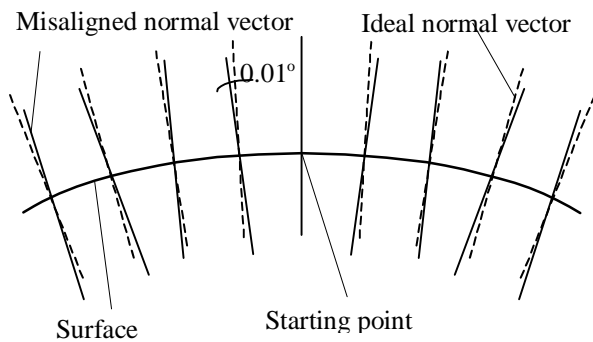
Fig. 9 (a)  $0.01^\circ$  (exaggerated) error to the right and left of the normal vector at the left and right of the starting point, and (b) its reconstruction error.

normal vectors at the left of starting point and  $-0.01^\circ$  for the normal vector at the right of starting point. This is the test of error if the orientation is coming from the left and right from starting point when the path of camera coming from the left and right of starting point.

The second set as shown in Fig. 9(a) contains error of  $-0.01^\circ$  for the normal vectors at the left of the starting point and  $+0.01^\circ$  for the normal vectors at the right of the starting point. This is the opposite test of error of the above orientation.

The third set as shown in Fig. 10 (a) contains error of  $+0.01^\circ$  and  $-0.01^\circ$  respectively for the left and the right normal vector from the starting point. This test is the combination of both orientations of normal vectors.

From these three sets of normal vector, their surface is reconstructed and their error is calculated by differentiating them to the ideal surface. The error is obtained as shown in Fig. 8(b), 9(b), and 10(b). This figures show that if every normal vector has the same orientation of error, the reconstruction error will be large. However, as shown in Fig. 10(b), if the orientation is opposite at two neighborhood normal vectors, the error is stable around some value. This is one example of normal vector data where the summation of error is zero. As the matter of fact, if the reconstruction is performed to a set of statistically random error normal vector, with the summation is zero, the error of reconstruction is stable around some value. It concludes that the propagation error does not occur in this method of reconstruction



(b)

Fig. 10  $+0.01^\circ$  (exaggerated) and  $-0.01^\circ$  error respectively for normal vector at the left and right of the starting point, and its reconstruction error.

### 3 Experiment

#### 3.1 Preparation.

In order to obtain surface normal vectors, we use five degrees of freedom mobile camera system. The camera is equipped with a LED which is attached on the camera axis and acts as the light source. Five degrees of freedom camera system is shown in Fig. 11. This system consists of a mobile camera, a movement control equipment, an image processor and a personal computer. The camera is attached on two rotary tables which are mounted on one of three linear stages in such a way that the camera can be moved along X, Y, and Z axes and also can be panned and tilted by computer control. The ray from the LED is reflected by the specular surface and caught by the camera. The image of the

reflected ray is analyzed by an image processor and a computer.

#### 3.1.1 Parallelization of Y Axis and the Camera Axis.

When the system is started, we don't know whether the camera axis is parallel or not to the Y axis since the zero value of the rotary table is not set to a certain coordinate. A procedure using a plane with a

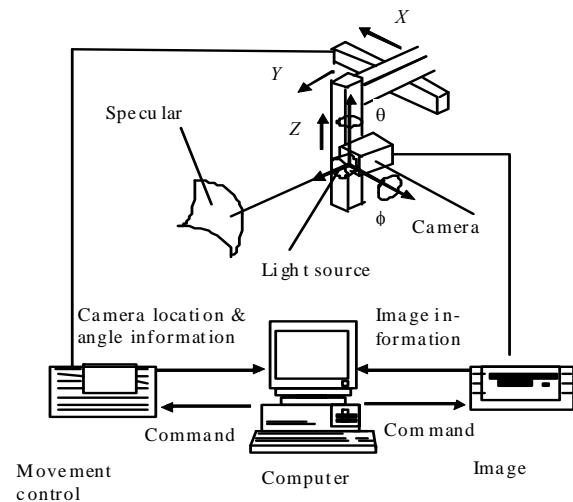


Fig. 11. Five Degrees of Freedom Camera System.

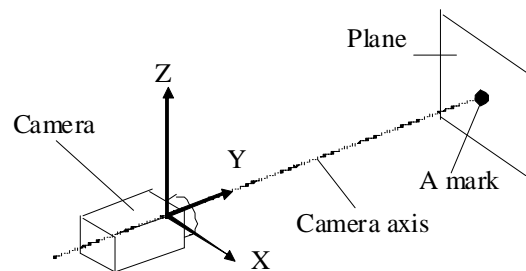


Fig. 12. Parallelization of the Y and the Camera Axis.

spot mark is performed to make the Y and camera axis parallel by moving the camera along the camera axis. (Fig. 12).

#### 3.1.2 Camera Scanning Path

As shown in Fig. 13, camera is moved in x and z axis from the starting point, however it must be panned and tilted if the object has a curved surface. The distance between camera and object



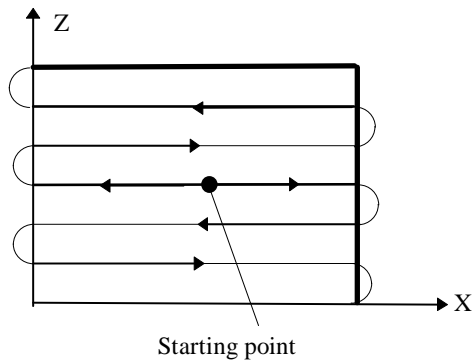


Fig. 13. Camera scanning Path in X-Z Plane.

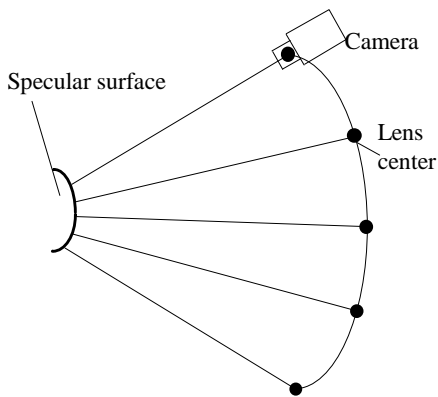


Fig. 14. Camera scanning Path in Y-Z Plane.

will change and the camera will not catch the reflected image if the path in Y-Z plane is not arranged. Therefore, after first movement, the distance of the camera to the object is calculated and the calculated distance is used for the next movement (see Fig. 14).

**3.1.3 Obtaining the Starting Point**

As shown in Fig. 15, the starting point is obtained by putting a spot on the object and measured the distance between the lens center and the spot mark by triangulation.

**3.1.4 Measuring the Convex Object with back surface reflection, and the Concave Object.**

The convex object of the next step has the characteristics of back surface reflection. In this case, the aligning of the reflected and incident ray

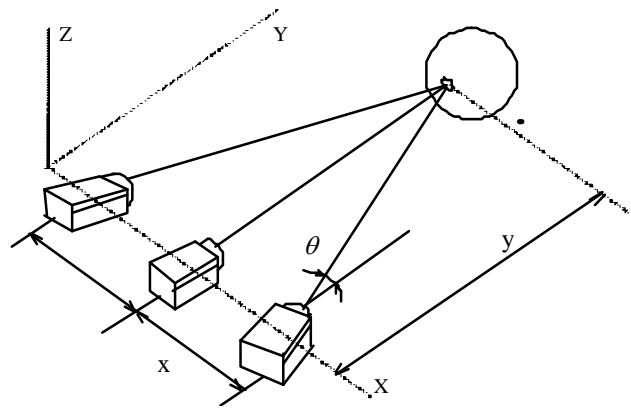


Fig. 15. Measurement of fixed point by triangulation.

will eliminate the effect of back reflection. As the matter of fact the back surface reflected ray also align with the incident ray. However, the gradients at the corresponding points on both surface should be parallel, otherwise we will have two kinds of the same intensity image. We can not distinguish and eliminate between the back surface image and the front surface image. Therefore, parallelism of the gradients at the corresponding points of both surface is the prerequisite (See Fig. 16).

The concave object of the next step is a concave mirror. The image of the light source should be a virtual image in the surface. If the radius is smaller than twice of the nearest distance ( that can be achieved by the camera with focus image) from the camera to the surface, the image will occur as real image and it needs more consideration in calculation and techniques. Therefore, at this stage we have the limitation that the radius should not be smaller than twice of the nearest distance from the camera to the surface (Fig 17).

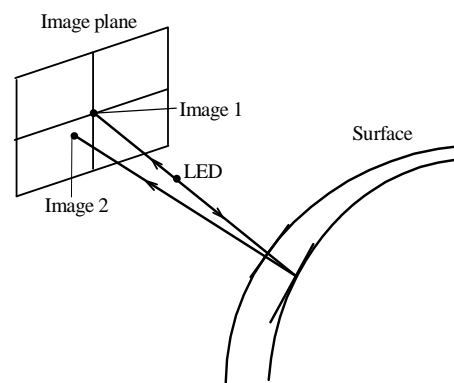


Fig. 16. The limitation of the thin glass

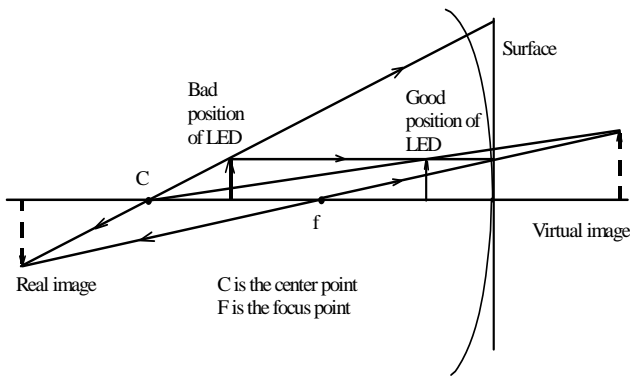
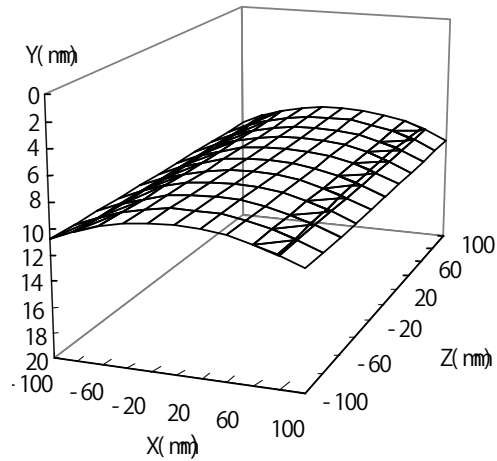


Fig. 17 The limitation of the concave object.



### 3.2 Experimental Result

We present here some of the experimental result that are a ball shape surface as the result of the previous work, an automobile glass window, and a radial concave mirror. The ball shape surface is a steel ball bearing surface with known radius. The radius of the ball is 75.000 mm. From this surface, 100 (10 x 10) data were scanned. Measurement were executed 10 times and the result are averaged. The average radius of the ball which was attained is 74.934 mm. The average error of the radius was 0.066 mm. Reconstructed shape of the ball is shown in Fig. 18.

The automobile glass window shows the ability of the system to measure a transparent thin(3.5 mm) and large size object. The distribution of error was obtained by a comparison with the contact measurement data using a matching program. We got a big maximum error, that was 167  $\mu\text{m}$ . This error may be distributed by the different set up between the contact measurement and this method.

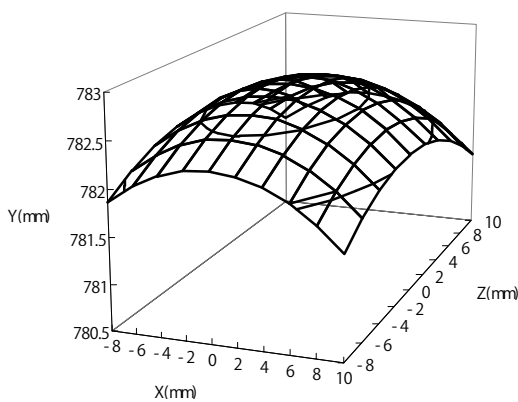


Fig. 18. Reconstructed Ball Shape Surface.

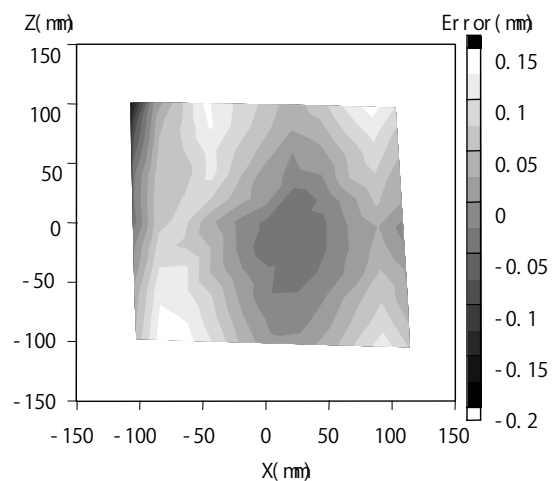


Fig. 19. Reconstruction of the Shape of the Automobile Glass Window and its Error Distribution.

The surface has a cylindrical form and has an elastic deformation. It's weight may deform the shape in the contact measurement since it was measured horizontally while this deformation did not occur when measured by our method vertically. Reconstruction of the shape of this object and its distribution of error is shown in Fig 19.

A concave mirror was used to check the ability of the method to measure the concave object. The object radius known as 1000 mm was used to check the result by comparing it to the reconstructed radius. We found that the maximum error was 5  $\mu\text{m}$ . The reconstructed shape of this object is shown in Fig. 20. (a) in the contour line and the distribution of error is shown in Fig. 20. (b).

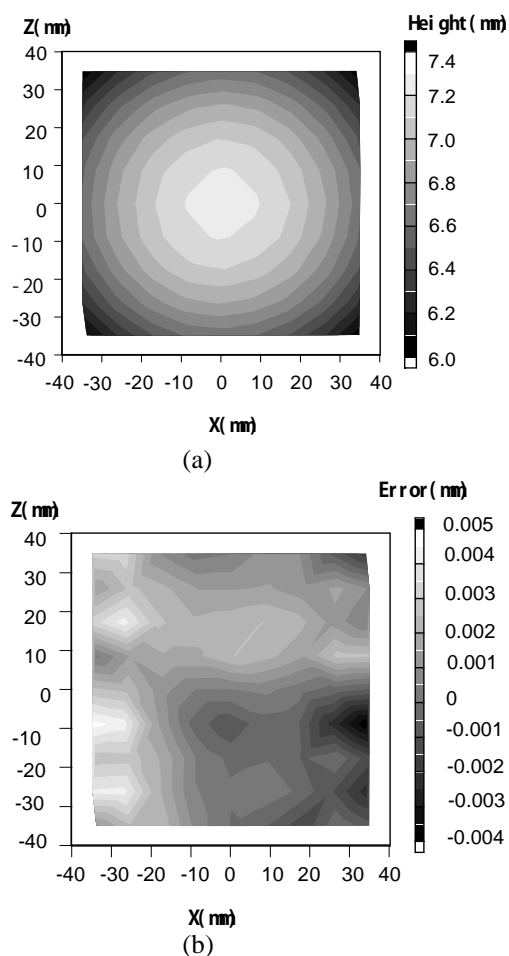


Fig. 20. Reconstruction of the shape of the concave mirror and error distribution.

#### 4 Conclusion

The new method of obtaining a 3D shape of specular surface by using five degrees of freedom (5-DOF) camera has been developed. This method uses normal vector to reconstruct the shape of the surface leading by a starting point of the surface. The normal vector is obtained by scanning the location and direction of the point on the surface by making the coincident condition of the incident ray on and reflected ray from the surface.

Present result have a good accuracy which are shown by a ball shape surface ( $66 \mu\text{m}$ ), automobile glass window ( $167 \mu\text{m}$ ), and concave mirror ( $5 \mu\text{m}$ ). More research and development is needed to achieve the better result especially for a large surface as automobile glass window. Both hardware and software equipment have their own source of error, however, the hardware development need other precision technology to make precise machine.

#### References:

- [1] K. Ikeuchi, Determining surface orientation of specular surfaces by using the photometric stereo, *IEEE Trans. Pattern Anal. Machine Intell.*, vol PAMI-3, Nov. 1981, pp 661-669.
- [2] A. C. Sanderson, L. E., Weiss, and S. K. Nayar, Structured highlight inspection of specular surface, *IEEE Trans. Pattern Anal. Machine Intell.*, vol PAMI-10, January 1988, pp 44-55.
- [3] M. D. R. Babu, C-H Lee, and A. Rosenfeld, Determining plane orientation from specular reflectance, *Pattern Recognition*, vol. 18, no. 1, pp. 53-62, 1985.
- [4] H. Schultz, Retrieving Shape Information from Multiple Image of specular Surface, *IEEE Trans. Pattern Anal. Machine Intell.*, vol PAMI - 16, pp. 195-201, February, 1994.
- [5] M. Baba, T. Konishi, H. Handa, "Shape Measurement of Columnar Objects with Specular Surfaces by Slit Ray Projection method", *IEICE Trans. On Information And Systems*, Vol. J83-D-II, no. 8, pp 1773-1782, August 2000.
- [6] P. Edi. A Flow Control for a High Subsonic Regional Aircraft Exploiting a Variable Camber Wing with Hybrid Laminar Flow Control. *IASME TRANSACTIONS Journal on Fluid Mechanics and Aerodynamics*, Issue 6, Volume 2, August 2005, ISSN 1790-031X, page 927-936.
- [7] P. Edi. The Development of N-250 Military Version. *WSEAS TRANSACTIONS on Fluid Mechanics*, Issue 8, Volume 1, August 2006, ISSN 1790-5087, page 832-837.
- [8] P. Edi, Nukman Y. and Aznijar A. Y. The Application of Computational Fluid Dynamic (CFD) on the Design of High Subsonic Wing. *WSEAS TRANSACTIONS on APPLIED and THEORETICAL MECHANICS*, Issue 9, Volume 3, September 2008, ISSN : 1991-8747.
- [9] K. Jain, "Fundamental of Digital Image Processing", Prentice Hall, Inc, Englewood Cliffs, New Jersey, 1986.
- [10] B. K. P. Horn, Determining shape from shading, *in the Psychology of Computer Vision*, P. H. Winston Ed., New York, Mc Graw Hill, 1975.
- [11] Hald, A. *Statistics Theory with Engineering Application*, New York: John Wiley & Sons, Inc. 1965.